Chemical Geology 346 (2013) 149–161

Contents lists available at SciVerse ScienceDirect

Chemical Geology

journal homepage: www.elsevier.com/locate/chemgeo

Water diffusion in potassium-rich phonolitic and trachytic melts

Sara Fanara [a,*], Harald Behrens [a], Youxue Zhang [b]

[a] Institut für Mineralogie, Leibniz Universität Hannover, Callinstrasse 3, D-30167, Hannover, Germany
[b] Department of Earth and Environmental Sciences, The University of Michigan, Ann Arbor, MI 48109-1005, USA

ARTICLE INFO

Article history:
Accepted 21 September 2012
Available online 27 September 2012

Keywords:
Water diffusion
Phonolite
Trachyte
IR spectroscopy

ABSTRACT

Water diffusivity was investigated in phonolitic and trachytic melts containing up to 6 wt.% of dissolved water at temperatures between 1373 K and 1673 K for running time of 108 to 1186 s using the diffusion couple technique. The experiments were performed in an internally heated gas pressure vessel (IHPV) at pressures of 0.2 or 0.3 GPa and in a piston cylinder apparatus (PCA) at pressures between 0.5 and 2.5 GPa. A newly developed rapid heating and rapid quench device was used for short term experiments in the IHPV. Concentration profiles of hydrous species (OH groups and H_2O molecules) and total water (bulk water concentration as sum of OH and H_2O molecules) were measured along the cylindrical axis of the diffusion sample using IR micro-spectroscopy. The IR spectroscopic technique was calibrated using a set of samples with bulk water contents measured by Karl–Fischer titration. Electron microprobe traverses show no significant change in relative proportions of anhydrous components along H_2O profiles, indicating that our data can be treated as effective binary diffusion between H_2O and the rest of the silicate melt.

Bulk water diffusivity was derived from profiles of total water using a modified Boltzmann–Matano method as well as using fittings assuming a functional relationship between the total water diffusivity ($D_{H_2O_t}$) and the total water concentration ($C_{H_2O_t}$). The fitting of the profiles indicates that for phonolitic melt the water diffusivity is roughly proportional to water content. The following formulation was derived for the prediction of total water diffusivity (m^2/s) as a function of T (K) in the T-range of 1373 to 1673 K and $C_{H_2O_t}$:

$$\log D_{H_2O_t} = -7.11 - 2.07 \log C_{H_2O_t} - \frac{\left(4827 - 4620 \log C_{H_2O_t}\right)}{T}.$$

The experimental data are reproduced by this relationship with a standard deviation of 0.07 log units. Water diffusivity in trachytic melts is similar at the same conditions. A pressure effect on water diffusivity could not be resolved in the range 0.2 to 2.5 GPa for phonolitic or trachytic melts.

1. Introduction

Water is the most abundant volatile component in natural magmas. The water content strongly affects the physical and chemical properties of silicate magmas, such as viscosity, density and diffusivity, and, hence, it is a crucial parameter controlling magmatic processes from fluid–melt interaction to magma mingling and mixing and volcanic eruption (Shaw, 1963; Watson, 1981). The eruptive style of a volcano is controlled by the kinetics of volatile release and its effect on rheological properties of the magma. Fundamental processes are bubble nucleation and growth, which are strongly affected by water diffusion in the melt (Kerr, 1995; Toramaru, 1995; Navon et al., 1998; Proussevitch and Sahagian, 1998; Zhang, 1999; Liu and Zhang, 2000; Martel et al., 2000; Zhang and Xu, 2003, 2008). It is therefore essential for modeling of various volcanic and magmatic processes to broaden our knowledge on water diffusion in silicate melts.

The diffusion of H_2O in rhyolitic, basaltic, andesitic and dacitic melts has been extensively studied in the past (see review of Zhang and Ni, 2010). Diffusion of water in silicate melts is some orders of magnitude faster than Si and Al diffusion but it is slower than diffusion of fast elements such as sodium and lithium (Watson, 1994). For volatile components, H_2O diffusion is faster than CO_2, SO_2, Ar, Kr and Xe but slower than He, H_2, and Ne (Behrens, 2010; Zhang and Ni, 2010; Zhang et al., 2010). So, for a given time, H_2O can migrate deeper into a contiguous melt than most other volatile components except for He, Ne and H_2. At the same time, dissolved water reduces the melt viscosity and enhances diffusion of slow elements.

In silicate melts and glasses the total water is dissolved at least in two hydrous species: OH^- groups and H_2O molecules (H_2O_m). It is important to considerer the role of speciation in diffusion because H_2O_m and OH^- possess different diffusivities. For polymerized melts such as rhyolite it is meanwhile accepted that molecular H_2O is the

* Corresponding author. Tel.: +49 5117625280; fax: +49 5117623045.
E-mail address: s.fanara@mineralogie.uni-hannover.de (S. Fanara).

0009-2541/$ – see front matter © 2012 Elsevier B.V. All rights reserved.
http://dx.doi.org/10.1016/j.chemgeo.2012.09.030

mobile species while OH^- groups are immobile (Zhang and Ni, 2010). For depolymerized melts such as dacite and possibly basalt, there is indication that hydroxyl groups may also contribute significantly to the diffusive transport of water (Behrens et al., 2004). In order to get deeper insight into the mechanisms of water diffusion, it is helpful to measure water species concentrations after diffusion experiments. This may allow constraining individual diffusivities of H_2O_m and OH^- groups (Zhang et al., 1991). However, unless the experimental temperature is low enough (e.g., ~773 K but depending on the water content and melt composition), concentrations of H_2O_m and OH^- groups in quenched melts do not represent the experimental conditions but speciation was frozen in at the glass transition (Dingwell and Webb, 1990; Zhang et al., 1995). Hence, information about the speciation at experimental conditions is often not available.

The aim of this work is to study water diffusion in phonolitic and trachytic melts at high temperature and pressures. Phonolite and trachyte are silica rich effusive rocks presenting high viscosity magmas with high degree of fragmentation during eruption, therefore producing some of the most powerful and destructive volcanic eruptions. Our experiments aim to provide data to quantify bubble growth and degassing in these eruptive systems. By combining our new data with previous results, we also attempt to discuss the mechanism of water diffusion and to describe its dependence on temperature and pressure.

2. Experimental and analytical procedures

2.1. Starting materials

As starting materials, synthetic analogs of potassium-rich phonolite and trachyte were made to match the phonolite whole rock composition of the Upper Lacher See Tephra (Smincke, 1997; Wörner and Smincke, 1984; Behrens and Hahn, 2009) and the composition of a trachyte from the basal unit of the Breccia Museo deposit from the Phlegrean Field (Italy) (Ricci, 2000; Freda et al., 2003; Di Matteo et al., 2004).

Dry glasses were synthesized by fusion of oxides and carbonates at 1873 K for 2 h in open platinum crucibles at ambient pressure in a conventional chamber furnace (Ohlhorst et al., 2001). To improve homogeneity, the quenched glass was crushed and melted again for another 2 h at the same temperature. The glass was finally rapidly quenched onto a brass plate.

The composition of glasses, displayed in Table 1, was analyzed by electron microprobe, Cameca SX100. The measurements were realized using 5 nA beam current, 15 kV accelerating voltage, a defocused beam with 20 μm in diameter and 8 s counting time with the exception of Na and K for which 2 s counting time was used to avoid alkali loss in particular for the wet samples. Composition of the phonolite is close to the natural analog while the synthesized trachyte has higher iron content compared to the natural trachyte. The ratio of non-bridging oxygen over tetrahedral cations (NBO/T) is close to zero for both anhydrous melts. In the calculation of NBO/T the Fe^{3+}/Fe_{total} ratios determined via colorimetry for air-melted glasses was used and Fe^{3+} was assumed to be a network former and Fe^{2+} a network modifier. The atomic ratio of Na/K is 1.32 for the phonolite and 1.09 for the trachyte.

Table 1
Composition of phonolitic and trachytic melts measured by electron microprobe.

Sample	Phonolite		Trachyte	
SiO_2	58.89	(42)	60.53	(39)
TiO_2	0.76	(2)	0.48	(4)
Al_2O_3	19.87	(19)	17.83	(24)
FeO[a]	3.61	(35)	7.14	(43)
CaO	3.90	(15)	1.72	(14)
MgO	0.69	(4)	0.21	(4)
Na_2O	5.96	(44)	5.22	(24)
K_2O	6.87	(25)	7.28	(19)
Total	100.55		100.45	
Na/K	1.32		1.09	
NBO/T	0.06		0.01	

Notes. Microprobe analyses are based on 30 measurements on three fragments of each glass. One standard deviation is given in parentheses.
Na/K = atomic ratio of alkali elements.
$NBO/T = (Na^+ + K^+ + 2\,Ca^{2+} + 2\,Mg^{2+} + 2\,Fe^{2+} - Al^{3+} - Fe^{3+})/(Si^{4+} + Ti^{4+} + Al^{3+} + Fe^{3+})$.
[a] All iron is given as FeO.

For preparation of hydrous samples, the obtained dry glasses were crushed and sieved to obtain two fine powder fractions with grain size of 200–500 μm and less than 200 μm. The two fractions were mixed in weight ratio of 1:1 to minimize the pore volume. The obtained mixture was loaded in $Au_{80}Pd_{20}$ capsules (30 mm length, 4 mm diameter, 0.2 mm wall thickness) and doped with doubly distilled water in several steps to improve the homogenization. The heating was carried out in an Internally Heated Pressure Vessel (IHPV) pressurized with Ar at 1473 K and 0.4 GPa for approximately 20 h. Oxygen fugacity is not controlled but is typically above NNO (Schuessler et al., 2008). Zhang and Ni (2010) showed that at 1373–1673 K molecular hydrogen diffusion does not significantly increase total hydrous component diffusivity as long as oxygen fugacity is higher than NNO-1. The samples were quenched isobarically, following a ramp (50 K/min to 673 K, 10 K/min from 673 to 573 K, 5 K/min to room temperature) defined to reduce the stress in the glass. The weight of each capsule was measured before and after annealing to test for possible leakage. Sample assemblages were always H_2O-undersaturated at experimental conditions so that water was completely dissolved in the melt and bubble-free glass pieces with water content ranging from 0.5 to 5.5 wt.% were obtained. Quench crystals were present in some of the synthesized glasses, but this is not a problem for the diffusion experiments since such crystals rapidly dissolve during heating to the target temperature. For the IR calibration a set of smaller samples (ca. 100 mg) was synthesized in an IHPV equipped with a rapid quench device (Berndt et al., 2002). Fast cooling prevented formation of quench crystals in this case.

2.2. Experimental techniques

2.2.1. Diffusion couple experiments in IHPVs

Diffusion couples consisted of two glass cylinders (3 mm length, 2.8 mm diameter) drilled out from the prepared dry and hydrous glasses and polished on one of the base planes. The two cylinders, having different water contents, were placed together with the polished surface in direct contact and loaded in Pt capsules. Each sample assemblage was prepared in a way to minimize air and free space in the capsule.

Water diffusion experiments in an IHPV at Leibniz University of Hannover were performed at 2 or 3 kbar pressure and temperatures from 1373 to 1677 K with run durations between 108 and 1188 s. For most of the IHPV experiments a new rapid heating–rapid quench device (RHQ) was used, as described below. For comparison, one experiment was run with a standard sample holder (NQ) heating the sample at a rate of 30 K/min and initial cooling at a rate of 100 K/min.

Rapid quench devices for IHPVs were developed and described in detail by Roux and Lefèvre (1992), Holloway et al. (1992) and Berndt et al. (2002). They were designed to prevent melts from crystallization during quench or any other quench effect. The new RHQ device used in this study (Fig. 1) was aimed to minimize the durations of both heating and cooling in the experiments. Thus, it is particularly useful for studying short term processes such as diffusion of fast species or viscous flow in low-viscosity melts. The sample is fixed with a ceramic glue (Ceramobond®) on a ceramic rod that has an iron wedge in the basal part. The ceramic rod is free to move in a ceramic tube between a storage position in the cold part of the oven and the

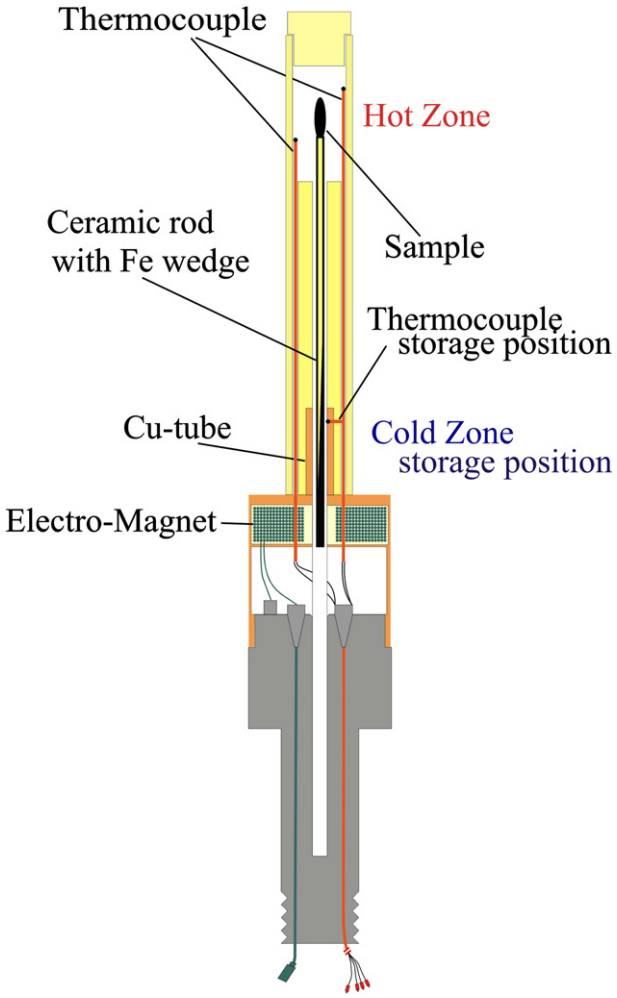

Fig. 1. Schematic cross section of the IHPV sample holder equipped with rapid heat–rapid quench (RQH) device. Ceramic parts are shown in yellow, steel in gray, brass and copper building units in brown, Teflon in light yellow, wires of the induction coil in green and thermocouples in red. Only two of the three thermocouples in the hot zone are displayed for clarity. The third thermocouple has its tip at intermediate height between the two ones shown. In this illustration the induction coil of the electromagnet is switched on, i.e. the sample is in the highest position. After switching of the power of the induction coil, the rod falls down to the bottom and the sample reaches the storage position.

experimental position. The cross section of the magnetizable wedge increases continuously over a length of 80 mm. At the beginning the upper end of the wedge just enters the lower part of an induction coil which is built by winding a coated 0.2 mm thick copper wire around a Teflon tube. After stabilization of temperature, the sample is moved within less than a second into the hot part of the furnace. The magnetic force of the induction coil (conditions 25 V and 1.9 A) allows lifting the ceramic rod by up to 7 cm, depending on sample load. Three S-type thermocouples are placed over a distance of 30 mm in the hot-zone of the furnace to measure the experimental temperature. Two of them are used to control the two heating loops of the furnace via a Eurotherm 2604 — controller/programmer (same furnace as described in Berndt et al., 2002). Temperature fluctuation in the hot zone was less than 3 K at the dwell (here the time between switching on and off the induction coil) and variation in temperature registered by the three thermocouples was less than 10 K. One S-type thermocouple is located near the storage position and provides information on the temperature change after fall of the sample. Even after fall of the sample from the highest temperature, the maximum temperature of this thermocouple was below 673 K. The pressure was automatically controlled within ±2.5 MPa during the whole experiment.

In the initial period of development of the setup we have used a movable rod with a flexible thermocouple connection to allow continuously monitoring the temperature at sample position. However, thermocouple reading was successful only in one experiment (Fig. 2), in all other attempts the thermocouple was disconnected from the recording system. Thus, we decided to simplify the setup to get better control on rod movement. The time–temperature curve in Fig. 2 indicates that the target temperature is reached within 20 s and cooling is almost instantaneous. Fitting the heating period by an exponential rate law indicate a temperature relaxation time of 6 s which is used to model the temperature evolution for the water diffusion experiments. Heating of gold wires placed inside a corundum tube in a platinum capsule confirmed this modeling of the time temperature path. Adjusting 1353 K at the two thermocouples controlling the heating loops, melting of gold wires was observed between 60 s and 90 s at 2 kbar (corresponding melting temperature of gold is 1349 K, Dinh Tam et al., 2010).

The time–temperature history of each experiment was recorded to estimate the contributions to the diffusion profiles due to the heating and cooling time. The effective run duration was calculated by:

$$t_{\text{eff}} = \int D_{T_{(t)}}/D_{T_{\text{final}}}\,dt = \int \exp\left(-E_a/R\cdot\left(1/T_{(t)} - 1/T_{\text{final}}\right)\right)dt \quad (1)$$

where $D_{T(t)}$ is the diffusivity at time t when temperature is $T(t)$, $D_{T,\text{final}}$ is the diffusivity at the target temperature T_{final}, E_a is the activation energy for diffusion, and R is the gas constant. For the RHQ experiments the heating path was modeled as $T_{(t)} = T_{\text{final}} + (T_{\text{initial}} - T_{\text{final}})\cdot\exp(-t/\tau)$ where T_{initial} (K) is the initial temperature and τ is the relaxation time (here 6 s). For cooling an initial rate of 150 K/s is estimated from Fig. 2.

2.2.2. Diffusion couple experiments in piston cylinder apparatus

A set of diffusion couple experiments was carried out in a piston cylinder apparatus (PCA) at the University of Michigan. The glass cylinders were prepared and placed together as described in Section 2.2.1. The Pt

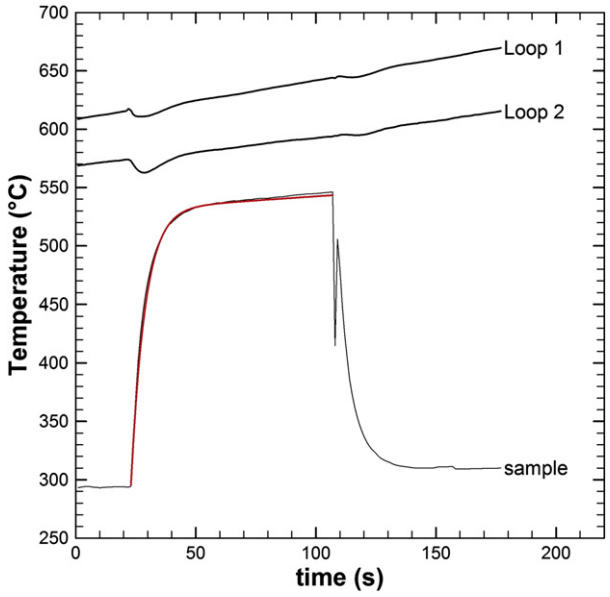

Fig. 2. Experimental time–temperature trend for diffusion couple experiment. The lines Loop 1 and Loop 2 refer respectively to the temperatures recorded at the upper and lower positions in the hot spot zone. The sample line records the temperature measured at the sample position. The sample's jump from the hot zone to the cold zone of the oven is represented by the peak during the cooling: in that moment the thermocouple was disconnected.

capsules were carefully closed to minimize air and free space. Each capsule was enclosed in a sample assemblage consisting in a $BaCO_3$ tube as the outer pressure medium and in a graphite heater and crushable alumina as the inner pressure medium. The diffusion couple was placed in the center of the graphite heater so that the interface was at the hottest point and the water-rich half was above the water-poor half. The temperature was measured on top of the platinum capsule using a type-D thermocouple.

A "piston out" procedure was used to bring the cold assemblage to the final pressure. The assemblage was initially over pressurized by circa 10 MPa and allowed to relax at 473 K for at least 2 or 3 h. Then the pressure was adjusted to the required one, and temperature was increased at a rate of 20 K/s or faster. Overshooting and fluctuation in temperature was <10 K. Runs at 1573 K lasted about 300 s, but also two 15 h runs at low temperatures (which crystallized) and two nominally "zero-time" experiments at 1573 K were run. Cooling was started by turning off the heating power resulting in an initial quench rate of circa 150 K/s. During the cooling, the pressure was held constant by manual pumping. After the run, the diffusion couple shows numerous cracks perpendicular to the cylindrical axis indicating non hydrostatic stress during cooling. A slower cooling rate in the final stage of cooling, with a rate of 100 K/s to 573 K and then 1 K/s to room temperature, did not prevent crack formation (Behrens et al., 2004).

To check redox changes at experimental conditions, six additional experiments were run in the PCA. Dry (synthesized in air) and hydrous (synthesized in an IHPV under intrinsic conditions) glass cylinders of 2.8 mm of diameter were drilled out from the prepared glasses and cut to a length of circa 5.00 mm. Sample assembly and run conditions were the same described above for the diffusion couple experiments.

The time–temperature history of each experiment was recorded to evaluate the effective run duration at the dwell temperature using Eq. (1). An average correction of 11 s needs to be added to the dwell duration to account for heating, cooling and overshooting. The correction time was calculated taking into account the time–temperature plots of the experiments and of the zero time experiments for each composition.

Error in temperature is fundamentally determined by sample setting: the thermocouple is in contact with the basal part of the capsule, therefore the measured temperature does not correspond with the real one at the capsule's center. To correct the temperature the distance of the thermocouple from the interface of the diffusion couple was measured, ranging typically from 3.0 to 3.5 mm (±0.2 mm). This value was compared with a calibration plot displaying ΔT (in K) versus the distance from the capsule's center (in mm), more details about the temperature uncertainty calculation can be found in Hui et al. (2008). Typically, a correction of 35 K needs to be added to the measured temperature. Temperature variation in the diffusion zone (±1 mm from the interface) is about 5 K.

A pressure correction is applied based on the calibration of the PCA at the University of Michigan by Hui et al. (2008) and Ni and Zhang (2008). The pressure correction of the PCA is about 6%.

2.3. Analytical techniques

Bulk water contents of hydrous glasses were measured by Karl–Fisher titration after thermal dehydration (Behrens et al., 1996). To test for the homogeneous distribution of water, two pieces of each glass block were analyzed. Differences in water content were typically below 5% relative. Raw data were corrected by adding 0.10 wt.% to account for unextracted water in glasses after heating (Leschik et al., 2004).

Doubly polished thick sections of post-experimental samples prepared for IR measurements were optically examined with a microscope to assure that the contact between the two halves was planar and perpendicular to the cylindrical axis, thus, that no significant convection was present in the melt during the experiments. Water contents of nominally dry glasses and water concentration–distance profiles in the samples after the experiments were detected by IR-microspectroscopy. IR spectra were collected with an IR microscope Bruker IR scope II connected to an FTIR spectrometer Bruker IFS88. Operation conditions were: light source, W lamp for NIR and globar light for MIR; beamsplitter, CaF_2 for NIR and KBr for MIR; detector, narrow band MCT with NIR equipment (range 600–10,000 cm^{-1}). To limit the volume of sample analyzed, a rectangular focus area of 30 μm wide and 100 μm long was chosen. Spectra were collected in 100 μm steps in the regions far from the transition surface, and in 50 μm to 30 μm as getting more close to transition plane. Typically 100 scans were accumulated for each spectrum, with a spectral resolution of 4 cm^{-1} for NIR and 2 cm^{-1} for MIR.

To evaluate the redox state of the melts, the relative abundance of ferrous and ferric iron was determined using a colorimetric method described by Schuessler et al. (2008). The air-melted trachyte and phonolite, the hydrous glasses synthesized in the IHPV and the series of 6 additional experiments run in the PCA (described in Section 2.2.2) were analyzed. For each measurement an amount ranging from 4 mg to 10 mg was used.

3. Results

3.1. Observation on post-experimental samples

The run products of diffusion experiments were checked for bubbles and crystals with an optical microscope, only the samples showing clear glasses were kept for further analyses, which mean that all experiments at subliquidus temperatures failed. Furthermore, the samples run at higher pressure in the PCA show fractures subparallel to the interface, attributed to shrinkage cracks during quench. Trachytic samples containing below 2 wt.% H_2O_t were not transparent even in thin sections due to a severe micro-crystallization of oxides.

The uncertainty in Fe^{3+}/Fe_{total} in the colorimetric data is quite large, therefore the results from these analyses will not be considered further on.

3.2. Major oxide concentration profile

Major oxide concentration profiles were determined by microprobe to test for contributions from other components to transport of water. Data points were collected along the same route used to determine the water concentration profile by NIR. No significant variations in the relative abundance of cations are visible (Fig. 3). Hence, the coupling of H_2O to other components was considered of minor importance and H_2O transport could be treated as binary inter-diffusion of H_2O and the rest of the silicate melt.

Microprobe analyses show also that extraction of iron from the melt into the platinum walls of the capsule was a minor problem in our experiments. In fact, the iron loss is restricted to just 200–300 μm along the capsules wall, being in our experiments the run duration short compared to the cation diffusion rates in the melt (Watson, 1982; Zhang et al., 1989; Zhang, 1993; Kress and Ghiorso, 1995; Koepke and Behrens, 2001; Behrens and Hahn, 2009; Zhang et al., 2010).

3.3. IR spectroscopy and description of diffusion profiles

Bulk water contents were determined in the MIR range from the peak height of the OH stretching vibration band of weakly H-bonded hydrous species at 3520 cm^{-1} (Scholze, 1959). In the NIR range, H_2O_m and OH^- contents were characterized respectively from the peak height of the H_2O stretching and bending band of H_2O molecules at 5200 cm^{-1} and from the peak height of the OH^-

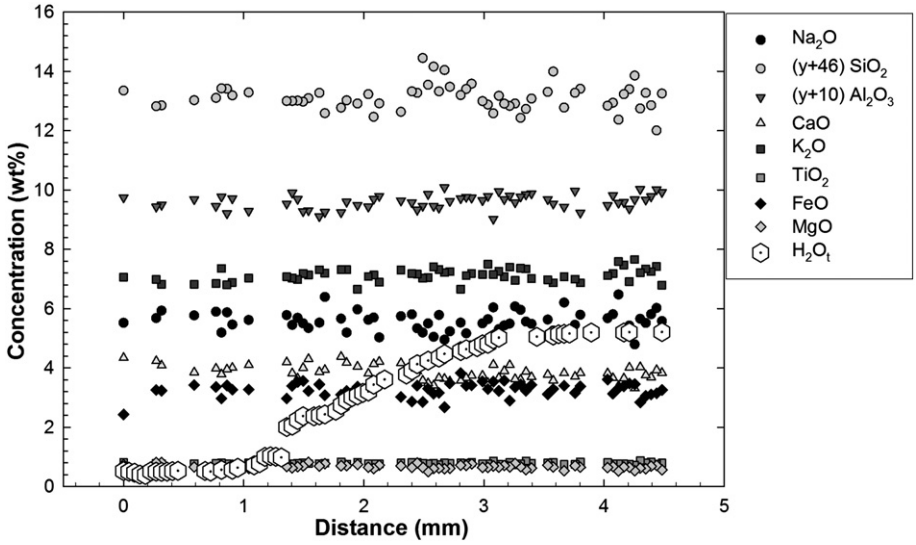

Fig. 3. Major oxide concentration profile for the sample P2 analyzed by electron microprobe along the cylindrical axis. Oxide contents are normalized to anhydrous composition to identify changes in relative abundance of cations. The H_2O_t profile is shown for comparison.

stretching and bending band of OH^- groups bounded with tetrahedral cations at 4500 cm^{-1} (Fig. 4a–b) (Stolper, 1982).

The Lambert–Beer law is the basis for a quantitative relationship between water concentration and the absorbance A (baseline-corrected height of the absorption peak):

$$C = MA/d\rho\varepsilon \tag{2}$$

where M is the molar mass of the component or species, d is the thickness of the sample in cm (measured by a Mitutoyo digital micrometer, accuracy ± 2 μm), ρ is the density in g/l, ε is the linear molar absorption coefficient in $l \cdot mol^{-1} \cdot cm^{-1}$ and C is the weight fraction in wt.%. As baseline, a tangent fitting the minima on both side of each band was used (Ohlhorst et al., 2001). For the fundamental OH stretching vibration band, the ε_{3550} values determined by Behrens and Hahn (2009) were used. Absorption coefficients for the NIR bands were calibrated in this study, using the density equations determined by Behrens and Hahn (2009) for phonolite [3] and trachyte [4],

$$\rho = 2512 - 11.4\, C_{H_2Ot}(\text{phonolite}) \tag{3}$$

$$\rho = 2457 - 24.0\, C_{H_2Ot}(\text{trachyte}) \tag{4}$$

where C_{H_2Ot} refers to the bulk water content of the glass. The terms C_{H_2Om} and C_{OH} are used to specify the concentration of water dissolved as water molecules and OH^- groups, respectively.

Assuming that no other hydrous species are present in the glass beside OH^- and H_2O ($C_{H_2Ot} = C_{H_2O} + C_{OH}$) and that the ε values do not vary with water content, the ε values can be determined using plots of absorbances normalized by density, thickness and water content (Behrens et al., 1996):

$$\left[\frac{1802 \cdot A_{5200}}{d \cdot \rho \cdot c_{H_2O_t}}\right] = \varepsilon_{H_2O} - \frac{\varepsilon_{H_2O}}{\varepsilon_{OH}} \cdot \left[\frac{1802 \cdot A_{4500}}{d \cdot \rho \cdot c_{H_2O_t}}\right]. \tag{5}$$

The values in brackets refer to the normalized absorbances for the peak at 5200 cm^{-1} and 4500 cm^{-1}. The relative uncertainty of the normalized absorbance increases with decreasing of water content, a direct consequence of the lower precision in measuring the peak heights and of the increasing of the relative error of KFT (Fig. 5). The molar absorption coefficients were determined by linear regression as the intercepts of the straight line with both axes.

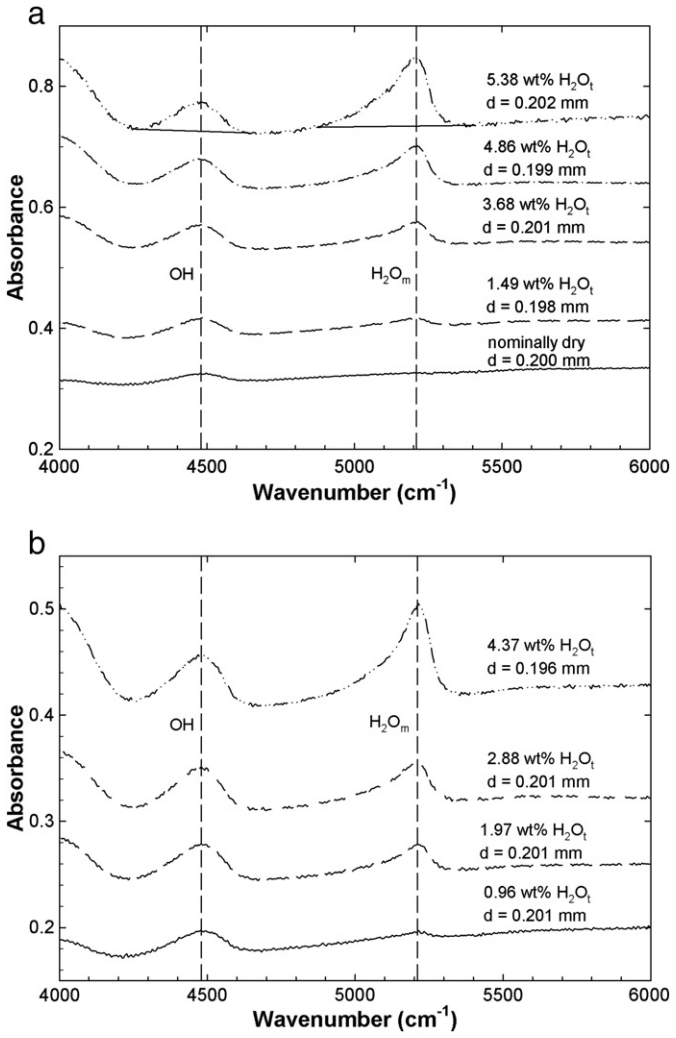

Fig. 4. a–b: Near infrared spectra of phonolitic (a) and trachytic (b) glasses with different amount of bulk water content. Thickness and water contents are displayed in the plots. The TT type baseline is shown for phonolite hydrous spectra with 5.38 wt.% H_2O_t. In the phonolite plot, the spectrum of a nominally dry glass is shown for comparison. Band assignments are: ~ 4500 cm^{-1} combination mode of OH^- groups; ~ 5220 cm^{-1} combination mode of H_2O molecules. Spectra are plotted with an offset for clarity.

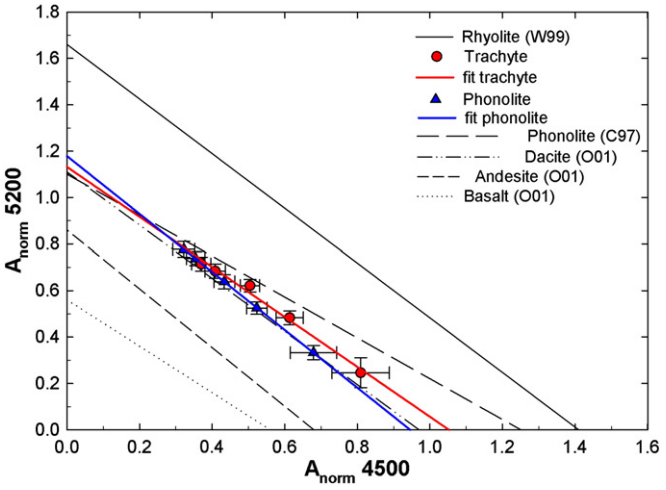

Fig. 5. Plot for determination of molar absorption coefficients for the OH combination band at 4500 cm^{-1} and H_2O combination band at 5200 cm^{-1}. Thick lines were obtained by the linear regression of the corresponding data in plot. Intercepts of the lines with the axes define the molar absorption coefficients for OH (x-axes) and H_2O (y-axes). For comparison data for dacite, andesite and basalt from Ohlhorst et al. (2001) [O01], data for rhyolite from Whiters et al. (1999) [W99] and data for phonolite from Carroll and Blank (1997) [C97] are shown. For all data the tangent baseline (Withers et al., 1999) was used to extract absorbances, except for those from Carroll and Blank (1997). The use of flexicurve baseline in that case results in higher absorption coefficient for OH band.

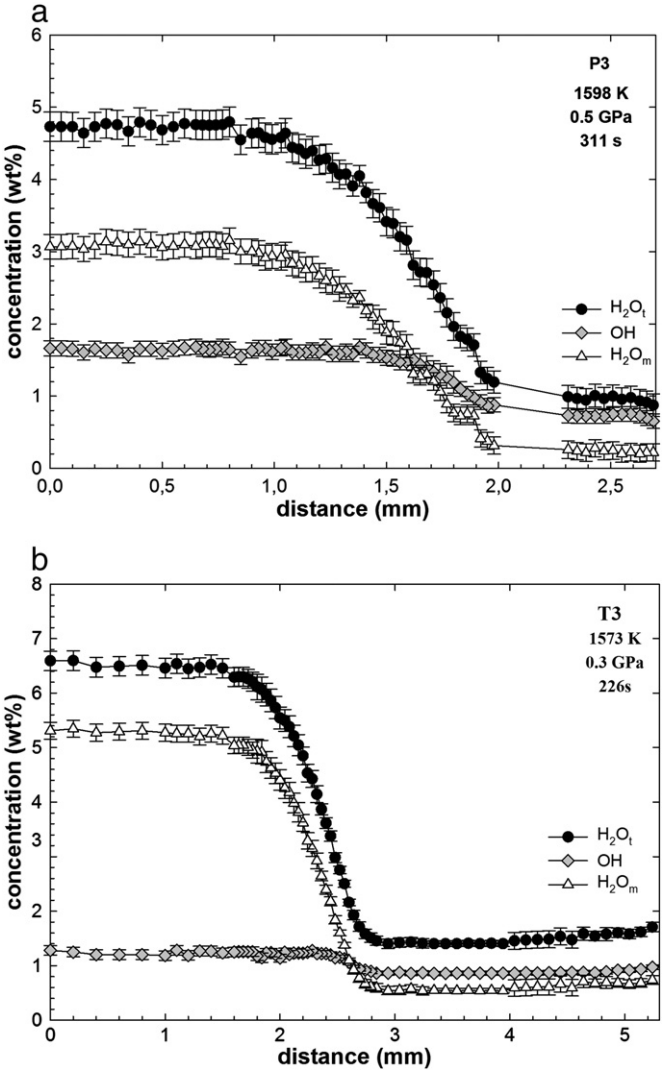

Fig. 6. a–b: Examples of concentration profiles of hydrous species and total water for phonolitic (a) and trachytic (b) samples. Black dots: bulk water content — gray diamonds: OH group — white triangles: molecular water. Error bars were calculated by error propagation considering error in thickness (0.002 mm), in the absorbance for peak at 4500 and 5200 cm^{-1} and in the density (0.02 g/l).

The resulting molar absorptivity coefficients for the combination band of OH^- at 4500 cm^{-1} are 0.94 ± 0.05 $L \cdot mol^{-1} \cdot cm^{-1}$ for phonolite and 1.05 ± 0.04 $L \cdot mol^{-1} \cdot cm^{-1}$ for trachyte. For the combination band of H_2O_m at 5200 cm^{-1} we determined absorption coefficients of 1.18 ± 0.03 $L \cdot mol^{-1} \cdot cm^{-1}$ for phonolite and 1.13 ± 0.02 $L \cdot mol^{-1} \cdot cm^{-1}$ for trachyte.

Comparing our results with data from previous studies (Fig. 5), it is evident that ε values systematically increase from basaltic to andesitic, to dacitic ≈ trachytic ≈ phonolitic, and finally to rhyolitic compositions. The slightly higher ε values reported for the phonolite composition of Carroll and Blank (1997) are probably due to differences in baseline determinations (a GG flexicurve was used) and in chemical composition.

Profiles of water dissolved as OH^- and as molecular H_2O are displayed in Fig. 6a–b. Consistent with previous studies (e.g., Silver et al., 1990; Behrens et al., 1996), OH^- groups are the dominating species at low water content. With increasing water content the OH^- group concentration approaches a constant value while molecular H_2O becomes the dominating species. As noted earlier, the relative abundance of hydrous species reflects conditions at the glass transition, and the glass transition temperature is lower as H_2O_t increases. At the high temperatures of the diffusion experiments the fraction of molecular H_2O is expected to be much smaller (Zhang et al., 1995, 1997; Withers et al., 1999; Nowak and Behrens, 2001). Since we do not know the equilibrium concentrations of hydrous species under experimental conditions, we have used the concentration–distance profiles of total water obtained by summing up both species concentration to model the diffusion process.

All successful diffusion experiments are summarized in Tables 2a–2b. In the dry part the concentration of dissolved water was often below the reliable range for the NIR combination band (<0.5 wt.%). In these cases, MIR analyses were used for the H_2O_t determination. Except for two samples (P1 and T8) pre- and post-experimental water contents agree within 0.5 wt.% or better. Such small differences may originate from inhomogeneities within the synthesized glass batches.

In order to extend the temperature range of the experiments, four dehydration experiments with phonolitic and trachytic compositions were performed at temperature of 773 K and 873 K, pressure of 0.2 GPa and with run duration ranging from 48 h to 15 h. However, these experiments failed because of partial crystallization.

For phonolitic melts a pressure effect on water diffusivity is not evident in the range of 0.5–2.5 GPa (Fig. 8). Due to experimental problems we don't have a systematic data set with pressure variation for trachytic melts in the PCA. Micro-crystallization of oxides was severe in all experiments with trachyte samples containing below 2 wt.% H_2O_t. Therefore, almost all the experiments including dry and 1 wt.% H_2O_t failed. The successful experiments on trachytic samples are listed in Table 2b. The diffusion couples run in the PCA show often numerous cracks. If the IR beam is on a crack or very close to it, the measured concentration of hydrous species is generally too low. Ignoring such data points the concentration–distance profiles can be constrained with acceptable quality. Diffusivity data from two experiments at 2.5 GPa are lower by a factor of 1.6 compared to IHPV experiments at 0.3 GPa (Table 2b), implying a decrease of water diffusivity with pressure. However, since the experiments were performed in two different apparatus at different redox conditions, and the difference is less than a factor of 2, the pressure effect on H_2O_t diffusion in trachyte melt is not well resolved from the experimental data. Hence, we will ignore the pressure effect in later discussion.

Table 2a
Results of water diffusion experiments for phonolite.

Sample	Composition	C_{H_2Ot} ini. (wt.%)	Pressure (GPa)	T (K)	Time (s)	Cooling	C_{H_2Ot} fin. (wt.%)	D_{water} at 1 wt.% H_2O ($\mu m^2/s$)	D_{water} at 3.5 wt.% H_2O ($\mu m^2/s$)	D_{water} at 1 wt.% H_2O ($\mu m^2/s$)
	Phonolite							Mod. Boltzmann–Matano method		Num. fitting
PHDC6	Phon. 0–5w	0.22/4.95	0.3	1677	228	RHQ	0.10/5.00	86 ± 17	293 ± 59	77 ± 4.1
P8	Phon. 0–5w	0.22/4.95	0.2	1673	225	RQ	0.18/4.50	91 ± 18	n.d.	85 ± 3.0
PHDC5	Phon. 0–5w	0.22/5.43	0.3	1673	108	RHQ	0.20/6.20	182 ± 36	474 ± 95	n.d.
P1	Phon. 0–5w	0.57/4.95	2.5	1598	311	RQ[a]	0.41/3.64	69 ± 14	n.d.	71 ± 4.5
P4	Phon. 2–5w	2.42/5.43	2.5	1598	311	RQ[a]	2.14/5.63	n.d.	184 ± 37	57 ± 1.8
P5	Phon. 2–5w	2.42/5.43	1.5	1598	311	RQ[a]	2.46/6.05	55 ± 11	93 ± 19	n.d.
P2	Phon. 0–5w	0.57/4.95	1.5	1598	311	RQ[a]	0.49/5.36	74 ± 15	n.d.	64 ± 1.9
P3	Phon. 0–5w	0.57/4.95	0.5	1598	311	RQ[a]	0.80/4.70	76 ± 15	n.d.	53 ± 1.5
PHDC2	Phon. 0–5w	0.22/5.43	0.3	1573	224	RHQ	0.30/5.70	70 ± 14	147 ± 29	n.d.
PHDC3	Phon. 0–5w	0.22/5.43	0.3	1573	108	RHQ	0.25/5.60	44 ± 9	184 ± 37	n.d.
PHDC4	Phon. 0–5w	0.22/4.95	0.3	1573	468	RHQ	0.18/4.10	68 ± 14	371 ± 74	72 ± 4.2
P6	Phon. 0–5w	0.22/4.95	0.2	1473	886	RQ	0.09/4.14	42 ± 8	n.d.	43 ± 0.7
P10	Phon. 2–5w	2.42/4.95	0.2	1473	886	RQ	2.49/4.46	n.d.	179 ± 36	59 ± 2.4
PHDC1	Phon. 0–5w	0.22/5.43	0.3	1473	323	NQ	0.14/5.80	n.d.	242 ± 48	n.d.
P9	Phon. 2–5w	2.42/5.43	0.2	1373	1186	RQ	2.02/5.32	n.d.	213 ± 43	n.d.
P7	Phon. 0–5w	0.22/5.43	0.2	1373	886	RQ	0.09/4.98	19 ± 4	n.d.	20 ± 0.8

[a] Samples run in the PCA; the other experiments were performed in the IHPV.

4. Discussion

4.1. Modeling water diffusion

Three methods were applied to fit concentration–distance profiles of H_2O_t to extract diffusion coefficients. On first instance, the profiles were fitted assuming a constant diffusivity. In second instance, a modified Boltzmann–Matano method was used. Finally, a functional relationship between diffusivity and water content was assumed.

4.1.1. Error function fit

Assuming a constant diffusivity D, the solution of Fick's second law for diffusion between two semi-infinite media with an initial concentration step at the interface is (Crank, 1975):

$$(C-C_{min})/(C_{max}-C_{min}) = 1-\mathrm{erf}\left[x/(4Dt)^{0.5}\right] \quad (6)$$

where C is the concentration at the distance x, C_{min} is the initial concentration in the dry half, C_{max} is the initial concentration in the hydrous half, and t is the time. None of the phonolitic samples are well reproduced by this fitting (Fig. 7a–b–e, dashed black curves). Four of the trachytic samples only show small deviations to such fitting while for the other trachytic samples the discrepancies are larger (Fig. 7c–d–f, dashed black curves). These findings are consistent with previous studies that water diffusivity often varies with water content in silicate and aluminosilicate melts (Zhang and Ni, 2010).

4.1.2. Modified Boltzmann–Matano method

The relationship between D_{H_2Ot} and C_{H_2Ot} was evaluated using the Boltzmann–Matano method modified by Sauer and Freise (1962):

$$D(x) = \frac{1}{-2t(\partial C/\partial x)_x}\left[(1-C_x)\int_x^{+\infty} C dx + C_x\int_{-\infty}^{x}(1-C)dx\right] \quad (7)$$

where C is the normalized concentration of H_2O_t:

$$C = (C-C_{min})/(C_{max}-C_{min}). \quad (8)$$

This approach has two advantages compared to the original method of Boltzmann (1894) and Matano (1932–1933): the position of the Matano interface does not need to be found and the precision is usually higher (Nowak and Behrens, 1997). To calculate the diffusion

Table 2b
Results of water diffusion experiments for trachyte.

Sample	Composition	C_{H_2Ot} ini. KFT (wt.%)	Pressure (GPa)	T (K)	Time (s)	Cooling	C_{H_2Ot} fin. NIR (wt.%)	D_{water} at 1 wt.% H_2O ($\mu m^2/s$)	D_{water} at 3.5 wt.% H_2O ($\mu m^2/s$)	D_{water} at 1 wt.% H_2O ($\mu m^2/s$)
	Trachyte							Mod. Boltzmann–Matano method		Num. fitting
T5	Trach. 1–6w	1.29/6.50	0.3	1673	226	RHQ	1.52/6.64	69[a]	208 ± 42	60 ± 1.3
T1	Trach. 0–5w	0.29/5.34	2.5	1598	311	RQ[b]	0.54/5.41	39 ± 7.8	n.d.	36 ± 1.2
T4	Trach. 2–5w	2.64/5.34	2.5	1598	311	RQ[b]	2.65/5.43	32[a]	95 ± 19	27 ± 2.0
T3	Trach. 1–6w	1.29/6.50	0.3	1573	225	RHQ	1.48/6.51	52[a]	155 ± 31	53 ± 0.7
T2	Trach. 2–5w	2.64/5.34	0.2	1473	886	RHQ	2.72/5.34	101[a]	304 ± 61	n.d.
T8	Trach. 1–6w	1.29/6.50	0.2	1473	466	RHQ	1.47/7.48	53[a]	158 ± 32	49 ± 1.3
T6	Trach. 2–5w	2.64/5.34	0.2	1373	886	RHQ	2.63/5.30	43[a]	129 ± 26	n.d.
T7	Trach. 1–5w	1.29/5.34	0.2	1373	466	RHQ	1.43/5.23	19[a]	56 ± 11	16 ± 0.8

Notes: Water diffusivities were determined using a modified Boltzmann–Matano method as well as using numerical fitting assuming water diffusivity being proportional to the water concentration. Initial water contents, $C_{H_2Ot,ini}$, were determined by KFT (>0.5 wt.%) or by MIR spectroscopy (<0.5 wt.%). Post-experimental water contents were measured by NIR (>0.5 wt.%) or by MIR spectroscopy (<0.5 wt.%). The two values reported refer to the halves of the couple. RQ: rapid quench; RHQ: rapid heat–rapid quench; NQ: normal quench. Error of the diffusion coefficients is estimated to be around 20% based on the quality of fit and on the uncertainty of experimental (T, P, t) and analytical (C_{water}, distance) parameters (Behrens et al., 2004).

[a] Extrapolation of data by Boltzmann Matano analysis down to 1 wt.% H_2O.

[b] Samples run in the PCA; the other experiments were performed in the IHPV.

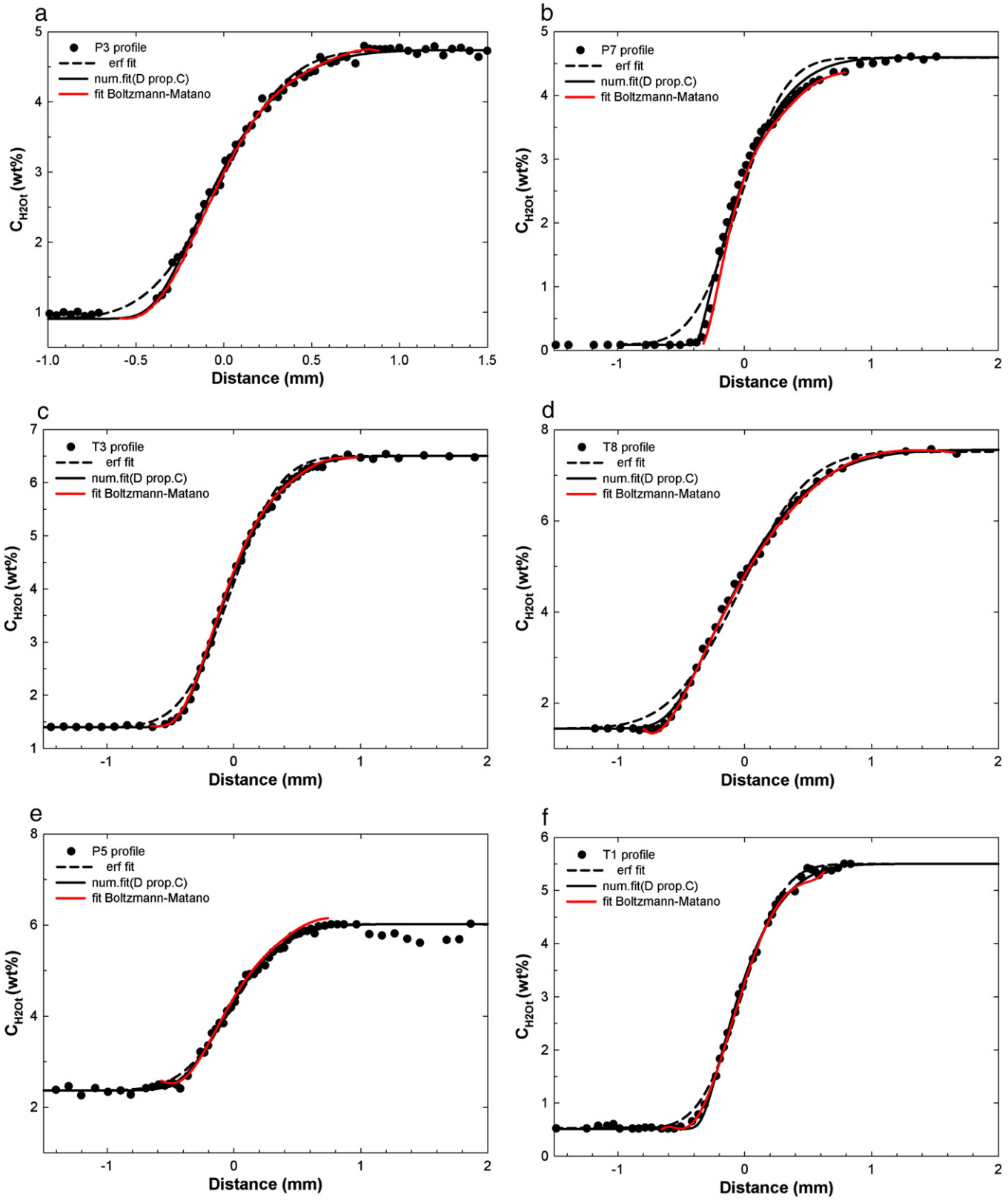

Fig. 7. a–f: Total water concentration profile of phonolitic and trachytic samples. Red solid curves are seventh-order polynomial fitting used in the modified Boltzmann–Matano method. Black dashed curves are error function fit assuming constant diffusivity. The solid black curves were fit assuming water diffusivity being proportional to C_{H_2Ot}.

coefficients by the Sauer and Freise (1962) approach, profiles were fitted for simplicity by seventh-order polynomials. It has to be emphasized that good fitting by such a polynomial can be only achieved when using a restricted range of the profile (see red lines in Fig. 7a–b–c–d). The profiles are well reproduced at intermediate concentrations, but systematic deviations of the fitted curve to the measured

data are noticeable at low and at high water concentration (Fig. 7e–f). These deviations have large impact on integrals and/or differentials in Eq. (7) and can produce sudden changes in slope of D_{H_2Ot} versus C_{H_2Ot}, as illustrated for run P3 (dotted triangles) in Fig. 8. In our experience, reliably diffusivity data can be obtained by the Boltzmann–Matano method only for normalized concentrations between 0.1 and 0.8 (see also Behrens et al., 2004). Except for run P3, diffusivity data are only plotted in this range in Figs. 8 and 9. The values of D_{H_2Ot} at 1, and 3.5 wt.% H_2O_t ($\mu m^2/s$) calculated by the modified Boltzmann–Matano method are listed in Tables 2a–2b and are displayed in Figs. 8 and 9. Despite of different pressure and different run duration, most of the data for phonolite show a linear dependence of D_{H_2Ot} on C_{H_2Ot} at intermediate water contents. Towards high water content a slight positive deviation from this trend is visible in Fig. 8. The onset of these deviations depends on initial water contents of both halves and, therefore, we attribute this phenomenon to imperfect fitting of the concentration–distance profile by the polynomial when the concentration curve flattens. The H_2O_t profile for run P5 is more scattered than those from other runs, especially at the high concentration end. As a result, the extracted D values have larger uncertainties. The deviations of these data to others at similar conditions are attributed to an insufficiently constrained concentration–distance curve for this particular sample and the diffusion data are not considered further on.

The diffusion profiles of trachyte samples successfully fitted by Boltzmann–Matano method are reported in Fig. 9b. Three sets of experiments with the same temperature and pressure but different H_2O_t range were used to test the reliability of the experiments (T1–T4; T2–T8; T6–T7 see Table 2b). Profiles of T2 and T6 show irregularities and the plateaus at high water content were not well developed. Therefore, the modified Boltzmann–Matano analysis based on polynomial fitting has large uncertainty. Only average diffusion coefficients could be determined which are listed in Table 2b. These data are higher than those for other samples at same conditions implying that T2 and T6 were affected by other transport processes such as convection. These runs will not be discussed further.

Experiments T1 and T4 were run at similar conditions, 1598 K and 2.5 GPa. In the water-rich part T1 contains numerous cracks which affects the measured water concentration profile so that the derived diffusivity data have some systematic error (Fig. 7f). Nonetheless, diffusivity data of T1 at low H_2O_t are in good agreement with the trend of data of sample T4. The sample T3 was run at lower pressure at 0.3 GPa and slightly lower temperature at 1573 K. T3 shows diffusivities more than half of a log unit higher than samples T1 and T4. This difference might be due to a pressure effect or experimental uncertainty.

4.1.3. Numerical fitting

The trends obtained by the modified Boltzmann–Matano analyses are roughly consistent with a linear variation of the water diffusivity with water content. For other natural melt compositions (rhyolite: Zhang and Behrens, 2000; Ni and Zhang, 2008; dacite: Liu et al., 2004; Behrens et al., 2004, Okumura and Nakashima, 2006; basalt: Okumura and Nakashima, 2006) proportionality between D_{H_2Ot} on C_{H_2Ot} was often found at least for low water concentrations. Therefore, in the third step the H_2O_t profiles were numerically fitted assuming

$$D_{H_2Ot} = C_{H_2Ot} * D_{(1\ \text{wt.\%})H_2O} \quad (9)$$

where is the bulk water diffusivity at 1 wt.% H_2O_t and C_{H_2Ot} is the water content in weight percent. The relationship originates from glass science literature (e.g., Doremus, 1973). Proportionality between D_{H_2Ot} and C_{H_2Ot} is expected if molecular H_2O is the mobile species and the diffusivity of H_2O molecules does not change with water content (Zhang and Stolper, 1991; Nowak and Behrens, 1997). In phonolitic samples, most profiles were well fitted by assuming D_{H_2Ot} proportional to C_{H_2Ot}. Only one sample (P7) presented some misfit indicating that D_{H_2Ot} increases more rapidly with H_2O_t content than predicted by the proportionality assumption. In trachytic samples, only two profiles (T3, T8) show a better fit by assuming D proportional to C, the other four profiles are more scattered and could be fit equally well using either this method or the error function fit (see solid black curves in Fig. 7a–b–c–d).

The values of D_{H_2Ot} at 1 wt.% H_2O_t ($\mu m^2/s$) calculated by numerical fitting are listed in Tables 2a–2b. For most phonolitic samples, these values and the ones calculated by the Boltzmann–Matano method are in good agreement, showing discrepancies lower than 11% relative and therefore within the experimental error (20%). Only for the samples P2 and P3 values of D_{H_2Ot} at 1 wt.% H_2O_t circa 30% relative higher were calculated by the modified Boltzmann–Matano method.

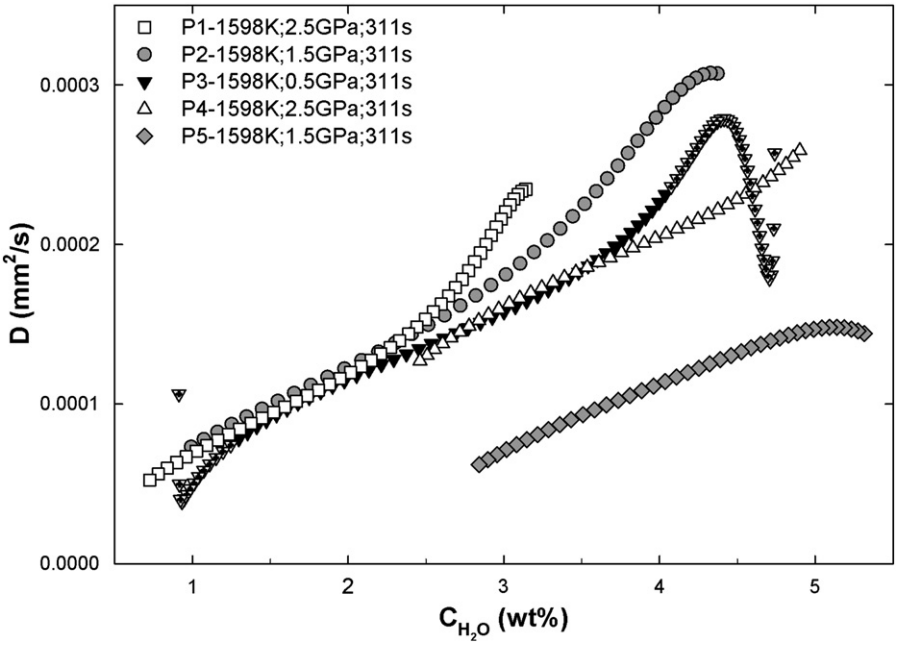

Fig. 8. Comparison D_{H_2Ot} vs. C_{H_2Ot} determined by Boltzmann–Matano analyses for phonolitic samples at different pressure: white symbols — 2.5 GPa; gray symbols — 1.5 GPa; black symbols — 0.5 GPa. For the sample P3, dotted triangles show the not reliable values. The experiments were performed in the PCA at T = 1598 K and t = 311 s. For details see text (Section 4.1.2).

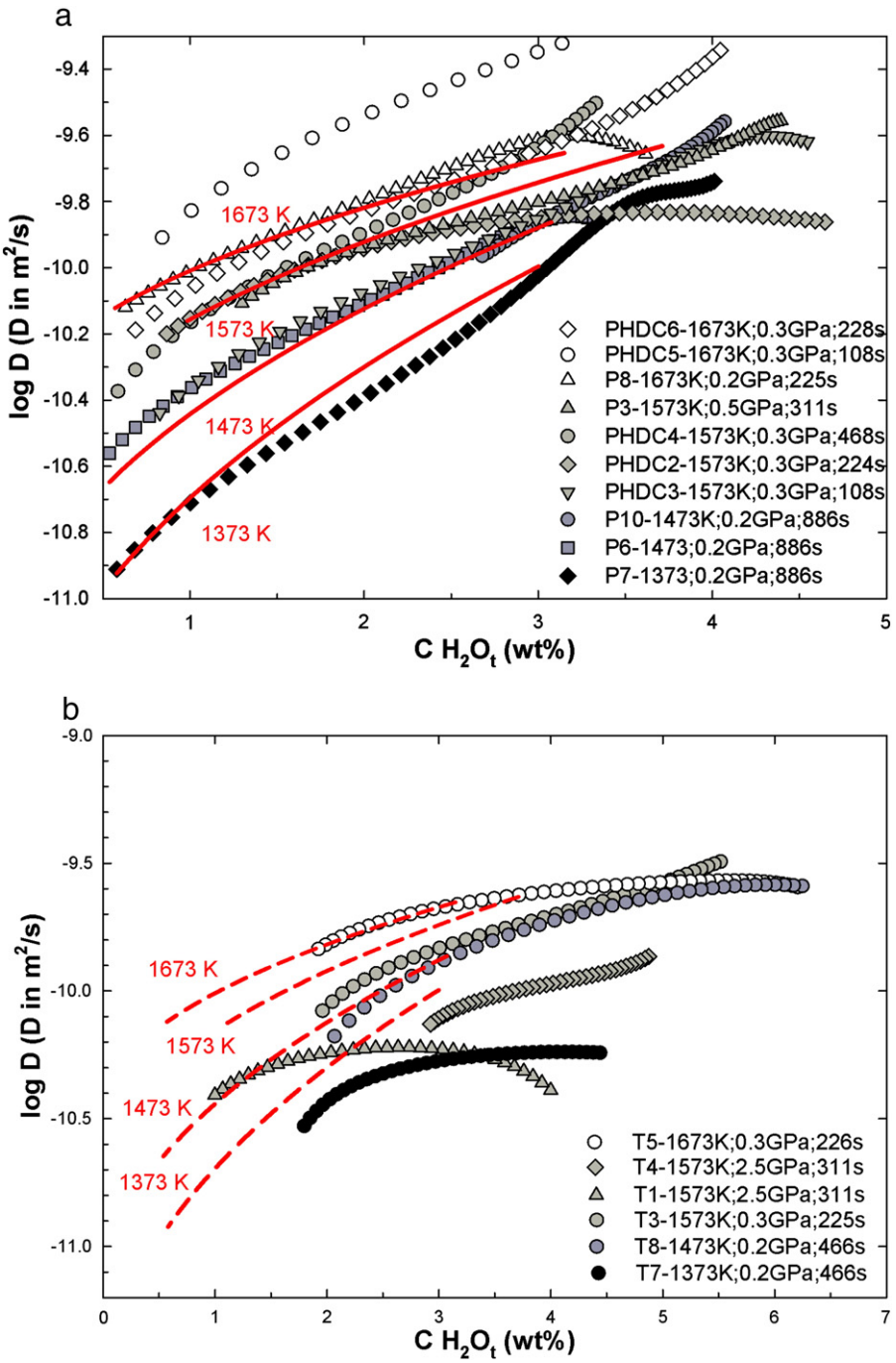

Fig. 9. a–b: Plot of log D_{H_2Ot} vs. C_{H_2Ot} for phonolitic (a) and trachytic (b) samples at different temperature based on Boltzmann–Matano fitting: white symbols — 1673 K; gray symbols — 1573 K; dark-gray symbols — 1473 K; black symbols — 1373 K. Diffusion trends for phonolitic melts at different temperatures obtained with the proposed model are plotted in red. In the trachytic plot (b), calculated diffusion trends for phonolitic melts are shown for comparison (dashed-red lines). For details see text (Section 4.2).

The water content of trachytic samples was usually >1 wt.% and, therefore, the water diffusivity at 1 wt.% H_2O was not directly accessible by the Boltzmann–Matano analysis. Using the diffusivities at 3.5 wt.% H_2O and assuming proportionality between D_{H_2Ot} on C_{H_2Ot}, extrapolated diffusivities for 1 wt.% H_2O are in very good agreement with the results of numerical fitting (Table 2b).

4.2. Diffusion equation for phonolite and trachyte

Using the data obtained by Boltzmann–Matano analysis, the following equation was derived for phonolitic samples to predict D_{H_2Ot} (m^2/s) as a function of T (K) and C_{H_2Ot} (wt.%) in the H_2O_t range of 0.5 to 3 wt.% and in the temperature range of 1373 to 1673 K at pressures below 0.5 GPa

$$\log D_{H_2Ot} = -(7.11 \pm 0.08) - (2.07 \pm 0.20) \log C_{H_2Ot} - \left[\left((4827 \pm 118) - (4620 \pm 306) \log C_{H_2Ot}\right)/T\right]. \quad (10)$$

This type of equation originates from the Arrhenius relation and was already used to describe the diffusivity of water in haplogranitic melts by Nowak and Behrens (1997). The experiments PHDC5 and

PHDC3 noticeably deviate from the other experiments (Fig. 9a) and were not considered to constrain Eq. (10). In both experiments the run duration was extremely short, and possibly the effective duration has been underestimated. The other experimental data at pressures up to 0.5 GPa are reproduced by this relationship with a standard deviation of 0.07 log units. Experiments at higher pressures of 1.5 and 2.5 GPa are in good agreement with Eq. (10) except for the sample P5 (see Section 4.1.2) indicating the water diffusion in phonolite melt is not sensitive to pressure in this range.

However, systematic deviations of experimental data from the fitting curves are evident in particular at high water contents (Fig. 9a). These deviations originate from the imperfectness of the Boltzmann–Matano analysis and are related in particular to the scatter in the concentration–distance profiles, as discussed above. We are aware that the derived relationship may have some systematic error in the exact description of the dependence of water diffusivity on water content and temperature, but it is nevertheless suitable to estimate for given water content and temperature the water diffusivity in phonolite melts within 30%. However, extrapolation out of the range of experimental determination may have significant higher error.

The activation energy based on Eq. (10) decreases from 119 kJ/mol at 0.5 wt.% H_2O to 50 kJ/mol at 3 wt.% H_2O, which is in good agreement with other melts (such as rhyolite to basalt, with typical activation energy of 40–160 kJ/mol, Zhang et al., 1991; Nowak and Behrens, 1997; Zhang and Ni, 2010).

Diffusivities of the trachyte were quite similar to those of the phonolite (see Fig. 10), but there is more scatter of data. Based on diffusivities obtained from three high-quality profiles (T3, T5 and T8), the difference between D_{H_2Ot} in trachyte and in phonolite is ≤35%, with slightly slower diffusivities in trachyte. Because there are not enough high-quality data to constrain the temperature dependence, and because of the similarity between trachyte and phonolite data, we suggest using Eq. (10) for rough estimation of D_{H_2Ot} in trachyte melt at 1373–1673 K.

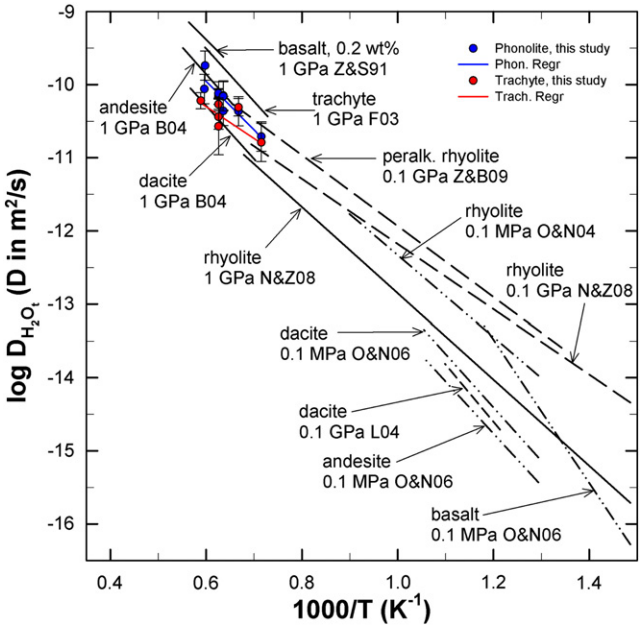

Fig. 10. Compilation of data for bulk water diffusivity in natural melts. Diffusion data are for 1 wt.% H_2O_t except for basalt (0.2 wt.% H_2O_t). Diffusivities in phonolitic melts were determined by a modified Boltzmann–Matano analysis. Diffusivities in trachytic melts are extrapolations down from the experimental range based on numerical fitting, assuming D_{H_2Ot} being proportional to C_{H_2Ot}. Data sources: basalt (Zhang and Stolper, 1991); rhyolite (Zhang and Behrens, 2000; Ni and Zhang, 2008); dacite at low T (Liu et al., 2004); trachyte (Freda et al., 2003); andesite and dacite (Behrens et al., 2004); dacite, andesite and basalt at low T (Okumura and Nakashima, 2006); peralkaline rhyolite (Behrens and Zhang, 2009).

4.3. Water diffusion in natural melts

In Fig. 10, water diffusivity at 1 wt.% H_2O_t as function of temperature for phonolitic (blue) and trachytic (red) melts at temperature ranging from 1373 to 1673 K and pressure between 0.5 and 2.5 GPa are shown in comparison to other natural melt compositions. The plotted diffusivity for phonolitic melts is based on the modified Boltzmann–Matano analysis. For trachytic composition, the plotted diffusivity is based on numerical fitting assuming D_{H_2Ot} being proportional to C_{H_2Ot}.

At a water content of 1 wt.% and temperatures above 1373 K, water diffusion systematically increases from rhyolite to dacite to andesite to basalt (Zhang and Stolper, 1991; Behrens et al., 2004; Ni and Zhang, 2008), with diffusivity in basalt being faster than in rhyolite by 1 to 1.5 log units. In other words, assuming absence of convection fluxes after 10,000 years at 1373 K water diffusion profiles in rhyolitic melts are relatively short, with diffusion lengths (defined as $x=(D_t)^{1/2}$) of 1.8 m, compared to those in basaltic melts, with lengths of 5.6 m.

At temperatures around 1073 and 1173 K, corresponding to the eruption temperature of silicic melts, only data for rhyolite and peralkaline rhyolite are available, with the water diffusion in peralkaline rhyolite being slightly faster than in rhyolite. Similar diffusivity than in peralkaline melts may be expected for phonolite and trachyte based on extrapolation of the high temperature data; however, this extrapolation has large uncertainty. At low temperatures near the glass transition the compositional trends invert because of higher activation energies for depolymerized melts compared to polymerized melts (Okumura and Nakashima, 2006). Thus, water diffusion in basalt becomes slower than in rhyolite. These temperature trends are only weakly affected by variations in pressure since the effect of pressure on water diffusion is typically small (Behrens et al., 2004; Ni and Zhang, 2008).

In the high temperature range, our data indicate slightly faster water diffusion in phonolite and trachyte than in rhyolite (Zhang and Behrens, 2000; Ni and Zhang, 2008). This is in agreement with the general pattern inferred from previous studies. Although the iron concentration in our trachyte is significantly higher, the obtained data fit in the trend showing diffusion values lower than in phonolite. On the other hand, our data for trachyte are at least 0.5 log units slower than reported by Freda et al. (2003), which show diffusivity values much higher than expected. The determined water diffusivity for phonolite is very close to that of the peralkaline rhyolite (Behrens and Zhang, 2009; Wang et al., 2009). This trend at high temperatures for hydrous melts is commonly explained with changing in the NBO/T values. However, in particular for alkaline melts, it cannot be excluded that other parameters, such as the total alkali content or the Agpaitic Index (defined as AI = Al–(K + Na)), could play an important role in the diffusion of H_2O_m or OH^- groups in the melt.

4.4. Water diffusing species

Strictly speaking, water diffusion in silicate melts is a complex multicomponent diffusion process (Mungall et al., 1998). However, often the anhydrous composition does not change along water diffusion profiles and the process can be treated as effective binary interdiffusion (Zhang and Ni, 2010). Diffusion of H_2O is strongly influenced by chemical and structural aspects of the silicate melts. Considering their structures, two types of melts can be distinguished: polymerized and depolymerized melts. In polymerized silicate melts the nominal ratio of non-bridging oxygens to tetrahedral cations (NBO/T) is close to 0. Melts of rhyolitic, peralkaline rhyolitic, trachytic and phonolitic and dacitic compositions belong to this group. Basaltic melts are considered to be depolymerized melts while andesitic melts have an intermediate state.

In both, polymerized and depolymerized melts, NIR and NMR spectroscopic studies have identified H_2O molecules and OH groups as hydrous species with the abundance of OH^- groups increasing

with total water content of the melt (e.g., Scholze, 1960; Stolper, 1982; Schmidt et al., 1999). In polymerized structures, i.e. rhyolite and dacite, it is generally accepted that molecular H_2O is the mobile species and hydroxyl groups do not contribute to bulk water diffusion (e.g., Zhang and Ni, 2010). To test whether this hypothesis also applies to trachytic and phonolitic melts, viscosity data are used to calculate diffusivities via the Eyring relationship:

$$D = (kT)/(\lambda\eta) \quad (11)$$

where k is the Boltzmann constant, λ is the jump distance and η is the viscosity. Basic assumption in this approach is that hydroxyl diffusion is controlled by structural relaxation of the melt. Assuming an effective jump distance of 3 Å (Behrens et al., 2004), and considering η = 910 Pa·s at 1573 K for a trachyte containing 0.88 wt.% of H_2O_t (Misiti et al., 2006) the estimated D_{OH} is 0.08 $\mu m^2/s$. For a phonolite of same composition as used in our study a viscosity of η = 710 Pa·s was determined for a melt with 1.89 wt.% of H_2O_t at 1323 K (Behrens and Hahn, 2009) corresponding to D_{OH} = 0.09 $\mu m^2/s$. In both cases D_{OH} is more than three orders of magnitude lower than bulk water diffusivity at same water content. Although OH^- diffusivity may not necessarily be the same as the Eyring diffusivity (Ni et al., submitted for publication, in revision, GCA), the calculations nonetheless support the dominant role of molecular H_2O in water diffusion in phonolite and trachyte.

In depolymerized melts other mechanism may contribute to the transport of water, depending on melt composition (Scholze and Mulfinger, 1959; Haider and Roberts, 1970; Zhang et al., 1991; Behrens et al., 2002, 2004; Xue and Kanzaki, 2004, 2006, 2008; Xue, 2009; Fanara and Behrens, 2011; Ni et al., submitted for publication).

5. Conclusion

Diffusivity of water was studied in phonolitic and trachytic melts at temperatures of 1373–1673 K and pressures up to 2.5 GPa. Diffusion profiles are roughly consistent with proportionality of D_{H_2Ot} on C_{H_2Ot} in the studied range of water contents. A simple Arrhenius-type equation is proposed to describe the water diffusivity in function of water content and temperature for phonolitic melts. A pressure effect could not be resolved for phonolite melts and thus the derive equation can be applied in the P-range of 0–2.5 GPa. Diffusion in trachytic melt is only slightly slower than in phonolitic melt, with difference no more than 35% (almost within experimental uncertainty), and hence may be roughly estimated by using the same expression. A small increase in the water diffusion coefficient from trachyte to phonolite is expected in the high temperature range due to higher degree of depolymerisation in phonolite, as indicated by the trend in water diffusivity from metaluminous rhyolite to peralkaline rhyolite and phonolite (Ni and Zhang, 2008; Behrens and Zhang, 2009).

High water diffusivities will enhance bubble growth in the melts and, hence, degassing will be more efficient in phonolitic and trachytic melts than in the rhyolitic melts. This can have influence on the eruptive style of a volcano. On the other hand one needs to consider that other parameters, as the viscosity and the decompression rate of the magma, also affect the power and the style of eruptions.

Due to the poorly constrained temperature dependence, extrapolation beyond the experimental range for both phonolitic and trachytic compositions is not recommended. Future studies should extend water diffusion experiments in phonolitic and trachytic melts at lower temperatures in order to develop a better data set of water diffusion at magmatic conditions. This would allow better modeling of magma degassing and other magmatic processes.

Acknowledgments

Sara Fanara acknowledges the Ministry of Science and Culture, Land Niedersachsen, for its support. The authors appreciate the help received from Jan Stelling, Marcus Oelze, Elke Schlechter, Francesco Vetere and Alex Bartels in projecting and constructing the RHQ-device. Sara Fanara thanks Huawei Ni for the support in preparing and running the experiments in the PCA at the University of Michigan. The authors thank Otto Dietrich for sample preparation.

References

Behrens, H., 2010. Ar, CO_2 and H_2O diffusion in silica glasses at 2 kbar pressure. Chemical Geology 272 (1–4), 40–48.
Behrens, H., Hahn, M., 2009. Trace element diffusion and viscous flow in potassium-rich trachytic and phonolitic melts. Chemical Geology 259 (1–2), 63–77.
Behrens, H., Zhang, Y., 2009. H_2O diffusion in peralkaline to peraluminous rhyolitic melts. Contributions to Mineralogy and Petrology 157, 765–780.
Behrens, H., Romano, C., Nowak, M., Holtz, F., Dingwell, D.B., 1996. Near infrared spectroscopic determination of water species in glasses of the system $MAlSi_3O_8$ (M = Li, Na, K): an interlaboratory study. Chemical Geology 128, 41–63.
Behrens, H., Kappes, R., Heitjans, P., 2002. Proton conduction in glass — an impedance and infrared spectroscopic study on hydrous $BaSi_2O_5$ glass. Journal of Non-Crystalline Solids 306, 271–281.
Behrens, H., Zhang, Y., Xu, Z., 2004. H_2O diffusion in dacitic and andesitic melts. Geochimica et Cosmochimica Acta 68, 5139–5150.
Berndt, J., Liebske, C., Holtz, F., Freise, M., Nowak, M., Ziegenbein, D., Hurkuck, W., Koepke, J., 2002. A combined rapid-quench and H_2-membrane setup for internally heated pressure vessels: description and application for water solubility in basaltic melts. American Mineralogist 87, 1717–1726.
Boltzmann, L., 1894. Integration der Diffusionsgleichung bei variablen Diffusionskoeffizienten. Annalen der Physik 53, 959–964.
Carroll, M.R., Blank, J.G., 1997. The solubility of H_2O in phonolitic melts. American Mineralogist 82, 549–556.
Crank, J., 1975. The Mathematics of Diffusion. Clarendon Press, Oxford, UK.
Di Matteo, V., Carroll, M.R., Behrens, H., Vetere, F., Brooker, R.A., 2004. Water solubility in trachytic melts. Chemical Geology 213, 187–196.
Dingwell, D.B., Webb, S.L., 1990. Relaxation in silicate melts. European Journal of Mineralogy 4, 427–449.
Dinh Tam, P., Duy, Tan P., Quang, Hoc N., Dinh, Phong P., 2010. Melting of metals copper, silver and gold under pressure. Proceedings of the National Conference on Theoretical Physics 35, 148–152.
Doremus, R.H., 1973. Glass Science. John Wiley, New York.
Fanara, S., Behrens, H., 2011. Proton conduction in hydrous glasses of the join $CaAl_2Si_2O_8$–$CaMgSi_2O_6$: an impedance and infrared spectroscopic study. Journal Chemical Geology 134.
Freda, C., Baker, D.R., Romano, C., Scarlato, P., 2003. Water diffusion in natural potassic melts. Geological Society of London Special Publication 213, 53–62.
Haider, Z., Roberts, G.J., 1970. The diffusion of water into simple silicate and aluminosilicate glasses at temperatures near the transformation range. Glass Technology 6, 158–163.
Holloway, J.R., Dixon, J.E., Pawley, A.R., 1992. An internally heated, rapid quench, high-pressure vessel. American Mineralogist 77, 643–646.
Hui, H., Zhang, Y., Xu, Z., Behrens, H., 2008. Pressure dependence of the speciation of dissolved H_2O in rhyolitic melt. Geochimica et Cosmochimica Acta 72, 3229–3240.
Kerr, R.C., 1995. Convective crystal dissolution. Contributions to Mineralogy and Petrology 121, 237–246.
Koepke, J., Behrens, H., 2001. Trace element diffusion in andesitic melts: an application of synchrotron X-ray fluorescence analysis. Geochimica et Cosmochimica Acta 65, 1481–1498.
Kress, V.C., Ghiorso, M.S., 1995. Multicomponent diffusion in basaltic liquids. Geochimica et Cosmochimica Acta 59, 313–324.
Leschik, M., Heide, G., Frischat, G.H., Behrens, H., Wiedenbeck, M., Wagner, N., Heide, K., Geißler, H., Reinholz, U., 2004. Determination of H_2O and D_2O contents in rhyolitic glasses using KFT, NRA, EGA, IR spectroscopy, and SIMS. Physics and Chemistry of Glasses 45, 238–251.
Liu, Y., Zhang, Y., 2000. Bubble growth in rhyolitic melt. Earth and Planetary Science Letters 181, 251–264.
Liu, Y., Zhang, Y., Behrens, H., 2004. H_2O diffusion in dacitic melts. Chemical Geology 209, 327–340.
Martel, C., Dingwell, D.B., Spieler, O., Pichavant, M., Wilke, M., 2000. Fragmentation of foamed silicic melts: an experimental study. Earth and Planetary Science Letters 178, 47–58.
Matano, C., 1932–1933. The relation between the diffusion coefficients and concentrations of solid metals (the nickel–copper system). Japanese Journal of Physiology 8, 109–113.
Misiti, V., Freda, C., Taddeucci, J., Romano, C., Scarlato, P., Longo, A., Papale, P., Poe, B.T., 2006. The effect of H_2O on the viscosity of K-trachytic melts at magmatic temperatures. Chemical Geology 235, 124–137.
Mungall, J.E., Romano, C., Dingwell, D.B., 1998. Multicomponent diffusion in the molten system K_2O–Na_2O–Al_2O_3–SiO_2–H_2O. American Mineralogist 83, 685–699.
Navon, O., Chekhmir, A., Lyakhovsky, V., 1998. Bubble growth in highly viscous melts: theory, experiments and autoexplosivity of dome lavas. Earth and Planetary Science Letters 160, 763–776.
Ni, H., Zhang, Y., 2008. H_2O diffusion models in rhyolitic melt with new high pressure data. Chemical Geology 250, 68–78.
Ni H. et al., submitted for publication. Geochemical and Cosmochemical Acta.
Nowak, M., Behrens, H., 1997. An esperimental investigation on diffusion of water in haplogranitic melts. Contributions to Mineralogy and Petrology 126, 365–376.

Nowak, M., Behrens, H., 2001. Water in rhyolitic magmas: getting a grip on a slippery problem. Earth and Planetary Science Letters 184, 515–522.
Ohlhorst, S., Behrens, H., Holtz, F., 2001. Compositional dependence of molar absorptivities of near-infrared OH^- and H_2O bands in rhyolitic to basaltic glasses. Chemical Geology 174, 5–20.
Okumura, S., Nakashima, S., 2006. Water diffusion in basaltic to dacitic glasses. Chemical Geology 227, 70–82.
Proussevitch, A.A., Sahagian, D.L., 1998. Dynamics and energetics of bubble growth in magmas: analytical formulation and numerical modeling. Journal of Geophysical Research 103 (B8), 18223–18251.
Ricci G., 2000. Il distretto vulcanico dei Campi Flegrei: petrologia e geochimica dei depositi di breccia e dei prodotti piroclastici associati. Ph.D. Thesis, University of Catania, Italy.
Roux, J., Lefèvre, A., 1992. A fast quench device for internally heated pressure vessel. European Journal of Mineralogy 4, 279–281.
Sauer, F., Freise, V., 1962. Diffusion in binären Gemischen mit Volumenänderung. Zeitschrift fur Angewandte Physik und Chemie 66, 353–363.
Schmidt, B.C., Holtz, F., Pichavant, M., 1999. Water solubility in haplogranitic melts coexisting with H_2O–H_2 fluids. Contributions to Mineralogy and Petrology 136, 213–224.
Scholze, H., 1959. Der Einbau des Wassers in Glaser. I. Der Einfluß des im Glas gelosten Wassers auf das Ultrarot-Spektrum und die quantitative ultrarotspektroskopische Bestimmung des Wassers in Glasern. Glastechnische Berichte 32, 81–88.
Scholze, H., 1960. Distinguishing between H_2O molecules and OH groups in glasses and minerals. Die Naturwissenschaften 47, 226.
Scholze, H., Mulfinger, H.O., 1959. Der Einbau des Wasser in Gläser. V. Die Diffusion des Wassers in Gläsern bei hohen Temperaturen. Glastechnische Berichte 32, 381–385.
Schuessler, J.A., Botcharnikov, R.E., Behrens, H., Misiti, V., Freda, C., 2008. Oxidation state of iron in hydrous phono-tephritic melts. American Mineralogist 93, 1493–1504.
Shaw, H.R., 1963. Obsidian-H_2O viscosities at 1000 and 2000 bar in the temperature range 700 to 900 °C. Journal of Geophysical Research 68, 6337–6343.
Silver, L.A., Ihinger, P.D., Stolper, E., 1990. The influence of bulk composition on the speciation of water in silicate glasses. Contributions to Mineralogy and Petrology 104, 142–162.
Smincke, H.U., 1997. Laacher See Tephra: Eruptionszentren, Eruptions- und Transportmechanismen. Nachrichten Deutsche Geologische Gesellschaft 11, 11–42.
Stolper, E., 1982. The speciation of water in silicate melts. Geochimica et Cosmochimica Acta 46, 2609–2620.
Toramaru, A., 1995. Numerical study of nucleation and growth of bubbles in viscous magmas. Journal of Geophysical Research 100, 1913–1931.
Wang, H., Xu, Z., Behrens, H., Zhang, Y., 2009. Water diffusion in Mount Changbai peralkaline rhyolitic melt. Contributions to Mineralogy and Petrology 158, 471–484.
Watson, E.B., 1981. Diffusion in magmas at depth in the Earth: the effect of pressure and dissolved H_2O. Earth and Planetary Science Letters 52, 291–301.
Watson, E.B., 1982. Basalt contamination by continental crust: some experiments and models. Contributions to Mineralogy and Petrology 80, 73–87.
Watson, E.B., 1994. Diffusion in volatile-bearing magmas. Reviews in Mineralogy 30, 371–411.
Withers, A.C., Zhang, Y., Behrens, H., 1999. Reconciliation of experimental results on H_2O speciation in rhyolitic glass using in situ and quenching techniques. Earth and Planetary Science Letters 173, 343–349.
Wörner, G., Smincke, H.U., 1984. Mineralogical and chemical zonation of the Laacher See Tephra sequence (East Eifel, W. Germany). Journal of Petrology 24, 836–851.
Xue, X., 2009. Water speciation in hydrous silicate and aluminosilicate glasses: direct evidence from ^{29}Si–^{1}H and ^{27}Al–^{1}H double-resonance NMR. American Mineralogist 94, 395–398.
Xue, X., Kanzaki, M., 2004. Dissolution mechanisms of water in depolymerized silicate melts: constraints from ^{1}H and ^{29}Si NMR spectroscopy and ab initio calculations. Geochimica et Cosmochimica Acta 68, 5027–5057.
Xue, X., Kanzaki, M., 2006. Depolymerization effect of water in aluminosilicate glasses: direct evidence from ^{1}H–^{27}Al heteronuclear correlation NMR. American Mineralogist 91, 1922–1926.
Xue, X., Kanzaki, M., 2008. Structure of hydrous aluminosilicate glasses along the diopside–anorthite join: a comprehensive one- and two-dimensional ^{1}H and ^{27}Al NMR study. Geochimica et Cosmochimica Acta 72, 2331–2348.
Zhang, Y., 1993. A modified effective binary diffusion model. Journal of Geophysical Research 98, 11901–11920.
Zhang, Y., 1999. A criterion for the fragmentation of bubbly magma based on brittle failure theory. Nature 402, 648–650.
Zhang, Y., Behrens, H., 2000. H_2O diffusion in rhyolitic melts and glasses. Chemical Geology 169, 243–262.
Zhang, Y., Ni, H., 2010. Diffusion of H, C and O components in silicate melts. Reviews in Mineralogy and Geochemistry 72, 171–225.
Zhang, Y., Stolper, E.M., 1991. Water diffusion in a basaltic melt. Nature 351, 306–309.
Zhang, Y., Xu, Z., 2003. Kinetics of convective crystal dissolution and melting, with applications to methane hydrate dissolution and dissociation in seawater. Earth and Planetary Science Letters 213, 133–148.
Zhang, Y., Xu, Z., 2008. "Fizzics" of bubble growth in beer and champagne. Elements 4, 47–49.
Zhang, Y., Walker, D., Lesher, C.E., 1989. Diffusive crystal dissolution. Contributions to Mineralogy and Petrology 102, 492–513.
Zhang, Y., Stolper, E.M., Wasserburg, G.J., 1991. Diffusion of water in rhyolitic glasses. Geochimica et Cosmochimica Acta 55, 441–456.
Zhang, Y., Stolper, E.M., Ihinger, P.D., 1995. Kinetics of the reaction $H_2O+O=2OH$ in rhyolitic and albitic glasses: preliminary results. American Mineralogist 80, 593–612.
Zhang, Y., Jenkins, J., Xu, Z., 1997. Kinetics of the reaction $H_2O+O=2OH$ in rhyolitic glasses upon cooling: geospeedometry and comparison with glass transition. Geochimica et Cosmochimica Acta 61, 2167–2173.
Zhang, Y., Ni, H., Chen, Y., 2010. Diffusion data in silicate melts. Reviews in Mineralogy and Geochemistry 72, 311–408.